PERGAMON

International Journal of Heat and Mass Transfer 45 (2002) 2077–2085

International Journal of HEAT and MASS TRANSFER

www.elsevier.com/locate/ijhmt

Numerical study of heat transfer in a laminar mist flow over a isothermal flat plate

V.I. Terekhov [a,*], M.A. Pakhomov [b]

[a] S.S. Kutateladze Institute of Thermophysics SB RAS, 1, Acad. Lavrent'ev Avenue, 630090 Novosibirsk, Russia

[b] Department of Technical Thermophysics, Novosibirsk State Technical University, 20, Karl Marx Avenue, 630092 Novosibirsk, Russia

Received 16 August 2001

Abstract

A model for predicting heat and mass transfer in a laminar two-phase gas–vapor–drop mist flow over a flat isothermal flat is developed. Using this model, a numerical study is performed to examine the influence of thermal and flow parameters, i.e., Reynolds number, flow velocity, temperature ratio, concentration of the liquid phase, and drop size, on the profiles of velocity, temperature, composition of the two-phase mixture, and heat-transfer intensification ratio. It is shown that, as the concentration of the liquid phase in the free flow increases, the rate of heat transfer between the plate surface and the vapor–gas mixture increases dramatically, whereas the wall friction increases only insignificantly.

Keywords: Heat and mass transfer; Drop evaporation; Numerical simulation; Laminar gas–drop flow

1. Introduction

Using, as heat carriers, two-phase gas–vapor–drop flows is one of the most effective means to intensify heat transfer. It is important, especially for technical purposes. that pronounced heat-transfer intensification can be achieved using rather low relative mass concentrations of the liquid. The mass content of the liquid phase is normally several percents; nevertheless, the heat-transfer rate can be increased by 5–8 times. Indications for this are experimental and numerical heat-transfer studies of mist-like flows around cylinders [1–3], wedges [4] and plates [5–7]. Similar effects were also reported for ducted flows, both laminar and turbulent, of vapor–drop [8,9] and gas–vapor–drop [10,11] mixtures.

The mechanism underlying the above phenomenon consists in using the latent heat of vaporization of liquid drops. However, the vaporization process depends on many thermal and flow parameters [8,9], which causes additional difficulties in theoretical treatment of ducted vapor–gas–drop flows or flat plate steam–gas–drop flows. To simplify the problem, many assumption were made, which has not allowed the authors of the above works to propose an adequate theory even for the physically simpler case of a laminar flow. This problem was addressed in more details in [7–12].

By now, detailed studies of ducted single-component vapor–drop flows over their hydrodynamically stabilized regions have been carried out [8,9]. Effect of a multitude of flow and particle parameters on heat-transfer intensification has been examined. Terekhov et al. [11] have considered a more complex case of heat and mass transfer in a developed two-component vapor–gas–drop flow. In their study, the longitudinal velocity profile was assumed to be automodel with allowance for the increased mass flow rate of the gas phase due to the vapor released by evaporating drops. This approach has allowed the authors to substantially simplify the problem so that there was no need to solve the equations of motion for the phase-carrier together with the energy and diffusion equations for the vapor–gas mixture.

Apparently, this approach cannot be applied to a two-phase boundary-layer flat plate flow or a flow over

* Corresponding author. Tel.: +7-3832-341736/328969; fax: +7-3832-343480.

E-mail address: terekhov@itp.nsc.ru (V.I. Terekhov).

0017-9310/02/$ - see front matter
PII: S0017-9310(01)00318-0

Nomenclature

Bi	Biot number
$b_{1D} = (K_{VS} - K_V)/(1 - K_{VS})$	diffusional injection parameter for the vapor released by an evaporating particle
$C_f/2$	skin friction coefficient
C_P, C_{pA}, C_{pL}, C_{pV}	heat capacities of mixture, air, liquid, and vapor J/(kgK)
D	vapor diffusivity in air (m^2/s)
d_L	drop diameter (m)
J_S	mass flux of vapor from the surface of an evaporating drop (kg/(m s))
K_A, K_V	mass concentrations of air and vapor in the binary vapor–air mixture
K_{VS}	mass concentration of vapor at the drop surface corresponding to saturation parameters at the drop temperature T_L
L	heat of vaporization (J/kg)
M_A, M_V, M_L	air, vapor, and liquid mass concentrations in the triple air-vapor-drops mixture
n	numerical density of drops (m^{-3})
Nu	Nusselt number
Nu_A	Nusselt number for a single-phase air flow
Nu_L	drop Nusselt number
Nu_P	Nusselt number of non-evaporating particle
Pr	Prandtl number
Re_x	Reynolds number calculated along the longitudinal coordinate
Re_L	drop Reynolds number
U, V	velocities in longitudinal/transverse directions (m/s)
$\bar{U}_i$	mean-mass flow velocity in current cross-section (m/s)
ΔU	relative velocity of the two phases (m/s)
Sc	Schmidt number
Sh	Sherwood number
St_D	diffusional Stanton number
T, T_L	mixture and drop temperatures (K)
x, y	coordinates (m)
X	plate length (m)
Δx	distance between calculation cross-sections along the longitudinal direction (m)

Greek symbols

α	heat transfer coefficient ($W/(m^2\ K)$)
β	mass transfer coefficient (m/s)
λ	heat conductivity (W/(m K))
μ	dynamic viscosity (Ns/m^2)
ν	kinematic viscosity (m^2/s)
θ	relative temperature profile
ρ, ρ_L, ρ_V	mixture, liquid, and vapor densities (kg/m^3)
τ	time (s)
ω	profile of nondimensional velocity

Subscripts

0	parameter under free-flow conditions
A	air
D	diffusional parameter
i	current calculation cross-section along the longitudinal coordinate
$i-1$	previous calculation cross-section along the longitudinal coordinate
L	drop
P	non-evaporating particle
S	parameter under saturation conditions
V	vapor
W	parameter under conditions at the wall
x	parameter calculated along the longitudinal coordinate

the initial length of a pipe. In this case, one has to solve the equations of continuity, momentum, energy, and the balance equations for flow components, together with certain appropriate relations at the interface between the phases. It is this problem which is considered in the present study.

Studies of laminar two-component mist flows are of obvious practical interest. Such flows are commonplace in miniature two-phase heat exchangers, especially in air conditioners, where, as a rule, the flow is laminar. This research field has been very scarcely addressed previously (see, [5–7,12,13]), and many questions in this problem still remain open. These questions, in particular, concern the influence of the liquid phase on the structure of the boundary layer, and also on heat and mass transfer in it, during variation of mass concentration and diameters of liquid drops and other parameters. In the present paper, results of a numerical heat-transfer study of a laminar boundary-layer mist flow over a flat plate are reported, and a comparison is made with available experimental data.

2. Problem statement

We consider a two-dimensional air flow, with liquid drops contained in it, over an isothermal flat plate with allowance for drop evaporation and vapor diffusion into air. The drops are assumed to be of identical diameters, and all other assumptions are the same as in [11]. We assume that the two-phase mixture flows without any substantial deposition of the drops onto the wall surface; consequently, no liquid film forms on the wall. Conductive heat transfer caused by immediate contact between the wall and drops and radiative heat transfer are ignored. At the pipe inlet, all particles have identical diameters and temperatures, and the number of particles in unit volume (the numerical concentration of particles) is also constant throughout the whole flow. The temperature of each drop is assumed to be uniform over its radius, since, according to [14], the Biot number is small, $Bi = \alpha_A d_{L0}/\lambda < 0.1$.

To model the momentum-, energy-, and mass-transfer processes in the gas–drops flow, we use the particle-source-in cell model (PSI-Cell) [15]. This model rests on the hypothesis according to which the drops acts as internal sources of the vapor mass, momentum, and energy in the gas phase. The mixture gives off heat to liquid drops, and the released vapor is heated to the main-flow temperature. The PSI-Cell model allows one to properly take into account the complex processes at the interface between the phases, which are characteristic of multiphase flows. Previously, Terekhov et al. [16] showed that this approach provides a good agreement with experimental data obtained by Mastanaiah and Ganic [10] for a ducted turbulent gas–drop flow.

In the calculations, we use a single-velocity approximation, validity of which is supported by the experimental data by Hishida et al. [5,6]. The LDA measurements performed by these workers showed that, under the conditions of interest, there is no substantial slippage between phases for particles 30–40 μm in diameter. It is assumed that no mixing between drops occurs in the radial direction; hence, the drop diameter varies in the transverse direction due to temperature variations across the boundary layer, causing the difference between the drop evaporation intensities at different radii.

3. Governing equations and numerical procedure

Under the above-indicated assumptions, the heat-transfer processes in the vapor–gas–drop flow can be described by the following system of the continuity, momentum, and energy equations for the vapor–gas mixture and the diffusion equation for vapor

$$
\begin{aligned}
&\varrho\left(\frac{\partial U}{\partial x}+\frac{\partial V}{\partial y}\right)+J_S\pi n d_L^2=0,\\
&\varrho\left(U\frac{\partial U}{\partial x}+V\frac{\partial U}{\partial y}\right)=\frac{\partial}{\partial y}\left(\mu\frac{\partial U}{\partial y}\right),\\
&\rho C_p\left(U\frac{\partial T}{\partial x}+V\frac{\partial T}{\partial y}\right)=\frac{\partial}{\partial y}\left(\frac{\mu C_p}{Pr}\frac{\partial T}{\partial y}\right)-\alpha\pi n d_L^2(T-T_L)\\
&\qquad\qquad+\rho D\frac{\partial K_v}{\partial y}(C_{pV}-C_{pA})\frac{\partial T}{\partial y},\\
&\varrho\left(U\frac{\partial K_v}{\partial x}+V\frac{\partial K_v}{\partial y}\right)=\frac{\partial}{\partial y}\left(\frac{\mu}{Sc}\frac{\partial K_v}{\partial y}\right)+J_S\pi n d_L^2.
\end{aligned}
\tag{1}
$$

As is seen, the continuity, energy, and diffusion equations in system (1) contain source (sink) terms due to the supply of the vapor mass from the particles and due to the heat flux from the mixture to the particles spent on their evaporation.

Relations (1) should be added with the equation of heat transfer at the interface between the phases

$$
C_{PL}\rho_L\frac{\pi d_L^3}{6}\frac{dT_L}{d\tau}=\alpha\pi d_L^2(T-T_L)-J_S\pi d_L^2\left[L+C_{pV}(T-T_L)\right],
\tag{2}
$$

and with the equation of conservation for the mass of the vapor released by evaporating drops [17]

$$
J_S=J_S K_{VS}-\rho_V D\left(\frac{\partial K_V}{\partial r}\right)_S.
\tag{3}
$$

Taking into account that the diffusional Stanton number is defined as

$$
St_D=-\rho_V D\left(\frac{\partial K_V}{\partial r}\right)_S\Big/\rho U(K_{VS}-K_V),
\tag{4}
$$

we may rewrite Eq. (3), with due regard for (4), in the form

$$
J_S=St_D U b_{1D},
\tag{5}
$$

where

$$
b_{1D}=(K_{VS}-K_V)/(1-K_{VS})
\tag{6}
$$

is the diffusional parameter for the vapor injection into the flow from the surface of an evaporating particle.

For finely dispersed particles, under the no-slip conditions ($\Delta U = U - U_L = 0$), the rate of mass transfer between the drops and the mixture is given by the following well-known relations [17]:

$$
Nu_P=\frac{\alpha_P d_L}{\lambda}=Sh=2
\tag{7}
$$

and

$$
St_D=Sh/Re_L\cdot Sc=2/Re_L\cdot Sc.
\tag{8}
$$

Then, Eq. (5) assumes the form [11]

$$
J_S=2D_{\varrho V}b_{1D}/d_L,
\tag{9}
$$

and the permeability parameter b_{1D}, which enters this equation, can be determined from Eq. (6) using the saturation curve.

The Nusselt number for the evaporating drops is given by the equation

$$Nu_L = \frac{\alpha d_L}{\lambda}. \tag{10}$$

According to [18], the quantity α in (10) is related to the coefficient of heat transfer toward the evaporating drops by the following formula:

$$\alpha = \frac{\alpha_P}{1 + C_p(T - T_L)/L}. \tag{11}$$

The material-balance equation for a binary vapor–air mixture has the form

$$K_V + K_A = 1. \tag{12}$$

For a triple mixture "vapor–gas–liquid", this equation is

$$M_V + M_A + M_L = 1. \tag{13}$$

The mass concentrations of the components of the mixture, K and M, may be written as

$$K_V = \frac{M_V}{M_V + M_A}, \quad K_A = \frac{M_A}{M_V + M_A} = 1 - K_V. \tag{14}$$

The expression for the current diameter of a drop in the ith calculation section is [16]

$$d_L i = \left[d_{Li-1}^2 - \left(d_{Li-1} - \frac{6 J_S \Delta x}{\overline{U}_{\rho L}} \right) \right]^{1/3}. \tag{15}$$

The boundary conditions used were the following.

At the inlet cross-section of the pipe

$$U = U_0, \quad T = T_0, \quad M_L = M_{L0}, \quad T_L = T_{L0},$$
$$d_L = d_{L0}, \quad K_V = K_{V0}. \tag{16}$$

At the external boundary of the boundary layer

$$M_L = M_{L0}, \ T_L = T_{L0}, \ d_L = d_{L0} \text{ and } \partial\Omega/\partial y = 0$$
for all other parameters. (17)

At the wall

$$T = T_W = \text{const}, \ U = V = 0 \text{ and } \partial\Omega/\partial y = 0$$
for all other parameters.

The local Nusselt number at constant wall temperature was determined from the temperature difference between the wall and the free flow

$$Nu_x = \frac{-(\partial T/\partial y)_W x}{(T_W - T_0)}. \tag{18}$$

To solve the system of equations obtained, a second-order accuracy finite-difference scheme along both directions was used, first proposed by Crank and Nicholson and described in detail in [19]. The obtained system of discrete equations was solved by the sweep method using the Thomas algorithm [19]. Since the main equations were nonlinear and conjugate equations, additional iterations along the longitudinal coordinate at each step were used. The length of the plate was $X = 0.2$ m. A total of 100 nodal points along the longitudinal directions and 50 nodal points along the crossflow directions were used. Besides, to check the calculation accuracy, test calculations on a finer grid were carried out (200×100 nodal points). The Nusselt number obtained in these calculations and the Nusselt number obtained on the coarser grid were found to be identical within 1%.

4. Numerical results and their discussion

All calculations were carried out for an air–water flow. The free-stream flow velocity was constant, $U_0 = 10$ m/s; the temperature was also unchanged, $T_0 = 293$ K; and the air–water mixture in the flow core was in its saturated state ($T_0 = T_{0S}$), so that the mass concentration of steam in the free flow was $K_{V0} = 0.014$. Thus, the following four parameters were varied in the calculations: Reynolds number ($Re_x = 10^3$–10^5), wall temperature ($T_W = 323$–473 K), mass concentration of the liquid phase ($M_{L0} = 0$–0.05), and drop diameter ($d_{L0} = 0.1$–100 μm). In the calculations, all drops in the free flow were assumed to have identical diameters, and the numerical concentration of particles remained unchanged throughout the flow studied: after their complete evaporation, the drops were treated as pseudoparticles of zero diameter.

Prior to the main calculation series, test calculations were performed for a ducted single-phase flow, and also for ducted steam–drop and steam–gas–drop flows over their hydrodynamically stabilized region. The largest difference between the numerical results obtained in this study and previously reported calculated values [8–11,16] was within 2.7%.

Primary attention in the next series of calculations was paid to revealing the influence of water concentration on the velocity and temperature profiles across the boundary layer. The predicted normalized velocity and temperature profiles along the automodel coordinate are shown in Fig. 1, where $\omega = U/U_0$ is the velocity profile (dashed curves); $\theta = (T_W - T)/(T_W - T_0)$ is the temperature profile in the steam–gas–drop flow (solid curve). In the absence of water, $M_{L0} = 0$, the predicted values were found to be coincident with the Blausius solution [20]. An increase in the water concentration makes the velocity profile to become more filled, due to intense evaporation processes taking place predominantly in the near-wall region. However, the water in the flow affects

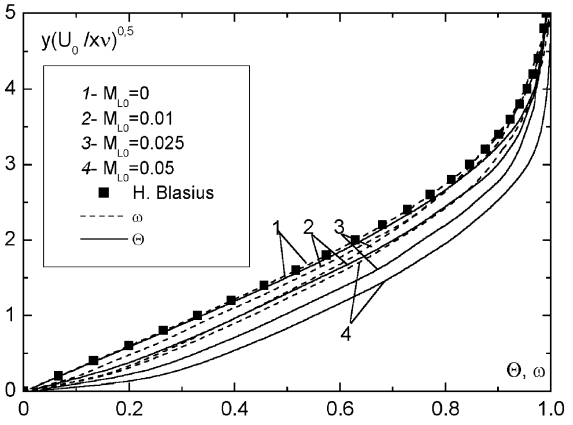

Fig. 1. Normalized velocity and temperature profiles across the vapor–gas–drop boundary layer flow. $Re_x = 5 \times 10^4$; $T_{L0} = T_0 = T_S = 293$ K; $K_{V0} = 0.014$; $d_{L0} = 30$ μm; $T_w = 373$ K.

the temperature profile in a greater extent, which should increase the heat-transfer rate more appreciably compared to friction. Indeed, as follows from Fig. 1, the thickness of the boundary layer is almost independent of the mass concentration of water in the flow.

The profiles of the concentrations of the flow components across the boundary layer drastically differ from the above-considered velocity and temperature profiles. The latter follows from Fig. 2, which depicts the mass-concentration profiles for steam and water. Since the plate surface is impermeable, the gradients of the concentrations of all substances here are zero.

Due to the evaporation processes, as we approach the wall, the mass concentration of water (Fig. 2(a)) continuously decreases. At certain values of water concentration in the flow core, M_{L0}, and of wall temperature, the near wall regions becomes free of drops, and a single-phase steam–air flow zone forms here. Apparently

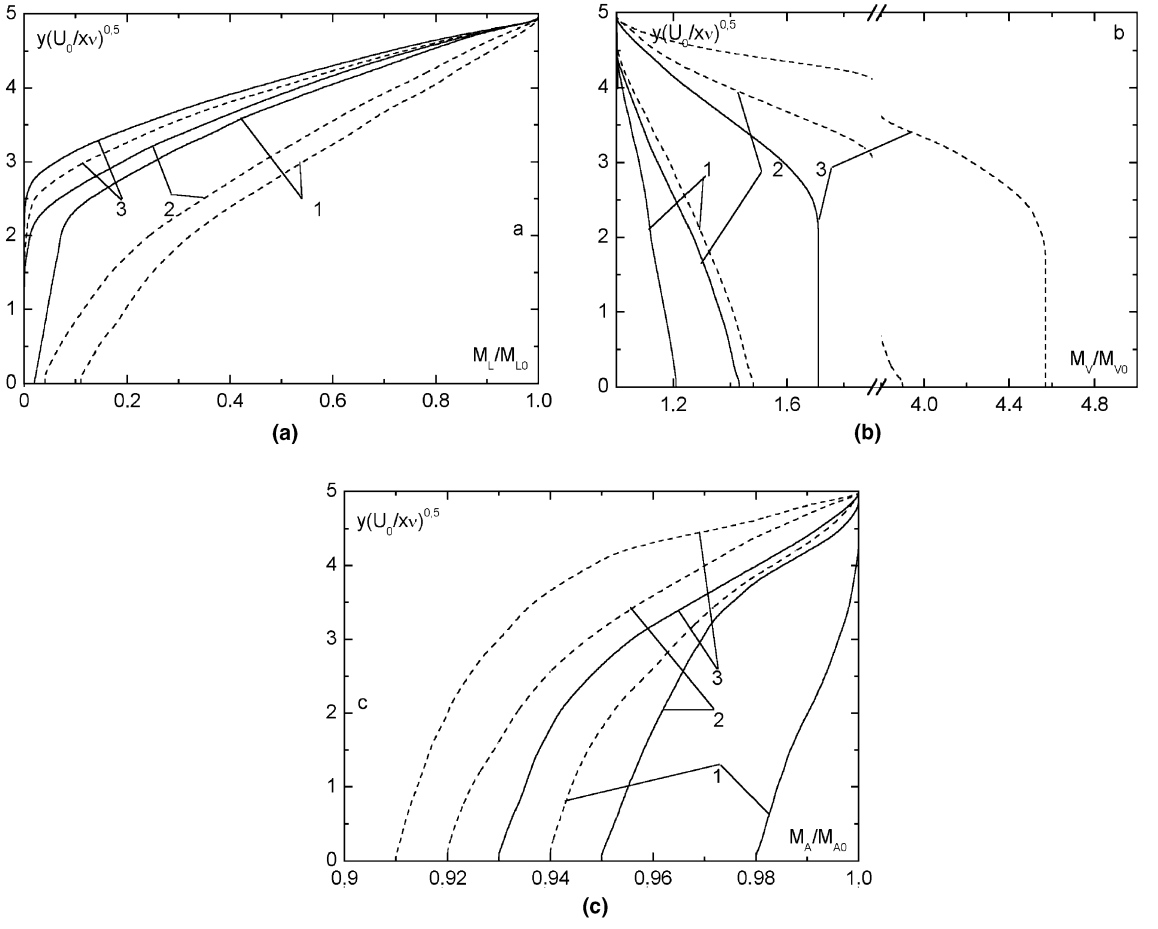

Fig. 2. Concentration profiles of the components of the two-phase mixture across the boundary layer: a – liquid phase; b – vapor; c – air. The experimental conditions are the same as for Fig. 1. Curve 1 – $T_W = 323$ K; curve 2 – $T_W = 373$ K; curve 3 – $T_W = 473$ K; solid curve – $M_{L0} = 0.01$; dashed curve – $M_{L0} = 0.05$.

(see also Fig. 2(a)), as the concentration of drops in the approaching flow decreases, the single-phase flow zone forms earlier, and its dimensions increase. The same regularity is also observed with increasing wall temperature.

With increasing wall temperature and water content in the flow, the steam concentration in the boundary layer also increases. The latter is clearly seen from Fig. 2(b), which shows that the rise in the steam concentration may be rather substantial.

For the conditions under study, with predominant air content in the approaching flow ($M_{A0} \approx 0.93$–0.98), it could be expected that the relative changes of air concentration in the flow would be small. This conclusion is supported by the numerical data shown in Fig. 2(c). The largest decrease in the air content near the wall, in the case shown, is below 10%; however, it may be expected that with increasing concentration of drops in the flow or with increasing wall temperature the air concentration near the wall should change more appreciably.

All peculiarities in the behavior of local characteristics of the steam–air–drop flow (Figs. 1 and 2) exert an influence the friction and heat-transfer rate. As is seen from Fig. 3, the presence of the liquid phase only insignificantly influence the friction coefficient. The latter well correlates with the data of Fig. 1, where a change in the water concentration had a weak effect on the fullness of the velocity profile. It should be also noted that the predicted dependencis for the friction coefficient for different concentrations of the liquid phase have identical slopes and for $M_{L0} = 0$ they coincide with the Blausius dependencies [20]:

$$C_f/2 = 0.332/Re_x^{0.5}. \tag{19}$$

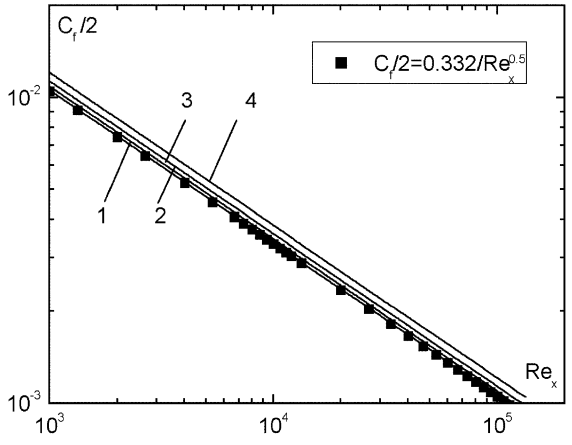

Fig. 3. Law of friction in the laminar vapor–gas–drop flow: curve 1 – $M_{L0} = 0$; curve 2 – $M_{L0} = 0.01$; curve 3 – $M_{L0} = 0.025$; curve 4 – $M_{L0} = 0.05$.

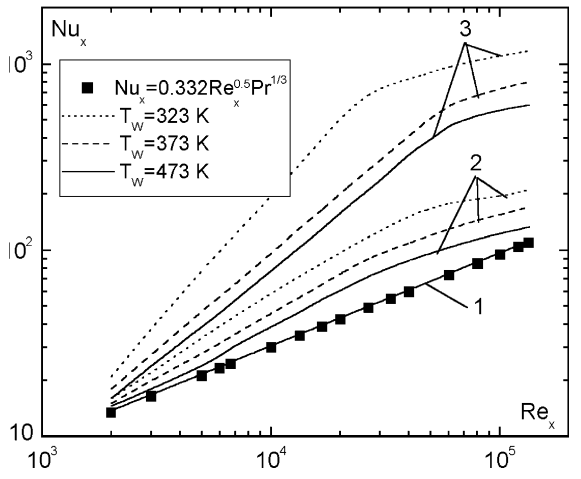

Fig. 4. Heat transfer in the laminar vapor–gas–drop flow: curve 1 – $M_{L0} = 0$; curve 2 – $M_{L0} = 0.01$; curve 3 – $M_{L0} = 0.05$.

For heat transfer, quite a different picture is observed (see Fig. 4). The liquid drops in the flow substantially enhance heat transfer. With increasing mass concentration of the liquid phase, the slope of the curves $Nu_x = f(Re_x)$ increases; further downstream, as the single-phase zone in the near-wall region widens, the slope approaches the standard law for laminar boundary-layer flow [20]:

$$Nu_x = 0.332 Re_x^{0.5} Pr^{1/3}. \tag{20}$$

Figs. 5 and 6 illustrate the effect of thermal and gasdynamic parameters of the two-phase flow on the heat transfer intensification ratio Nu/Nu_A, where Nu_A is the Nusselt criterion for an air flow with a mass velocity identical to that of the two-phase flow, all other conditions being also identical.

As follows from these figures, the heat transfer intensification ratio may be rather high (up to 10 times). Of course, the heat-transfer rate increases with increasing concentration of the drops. However, as follows from Fig. 5, the most pronounced heat transfer intensification is observed at low concentrations of the liquid phase, $M_{L0} < 0.01$–0.02. Further increase in the concentration of the liquid phase is of no substantial consequence; it seems therefore unreasonable to use such flows for raising the heat transfer rate in technical apparatus.

The wall temperature exerts a substantial influence on the heat transfer intensification ratio. As the temperature increases, the near-wall region rapidly gets free of the liquid phase; as a result, the heat transfer rate diminishes.

Another peculiarity in the behavior of the predicted data of Fig. 5 deserves mention. All other conditions being kept unchanged, an increase in the Reynolds number Re_x intensifies heat transfer. This tendency

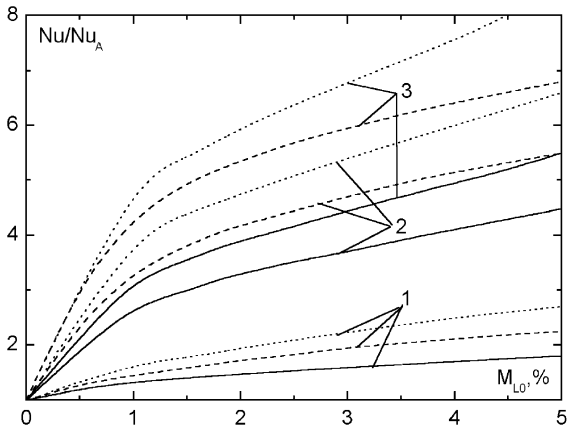

Fig. 5. Effect of liquid-phase concentration on the heat-transfer intensification ratio: curve 1 – $Re_x = 10^4$; curve 2 – $Re_x = 5 \times 10^4$; curve 3 – $Re_x = 10^5$. $U_0 = 10$ m/sec. Dot curves – $T_W = 323$ K; dashed curves – $T_W = 373$ K; solid curves – $T_W = 473$ K.

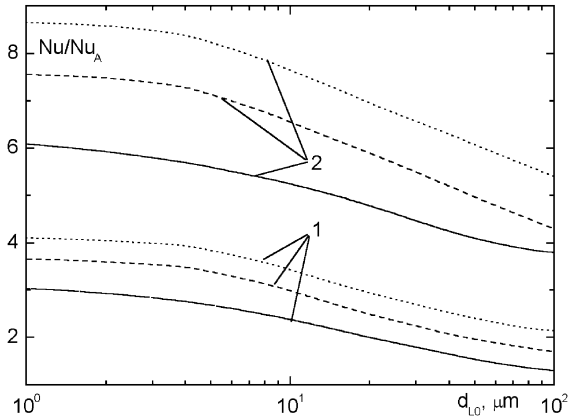

Fig. 6. Effect of drop diameter on local heat-transfer intensification: curve 1 – $Re_x = 10^4$; curve 2 – $Re_x = 5 \times 10^4$. $U_0 = 10$ m/sec. Dot curves – $T_W = 323$ K; dashed curves – $T_W = 373$ K; solid curves – $T_W = 473$ K.

shows up also for other flow conditions; the experimental studies [5,6] provide another indication for it.

The size of liquid drops in the approaching flow is one of the main parameters that determine heat- and mass-transfer intensity in two-phase flows. Numerical results concerning this dependence are shown in Fig. 6. With increasing diameter of the liquid drops, at their mass content in the flow kept unchanged, the surface area of the interface between the phases decreases. As a result, the heat-transfer rate also decreases. Simultaneously, small droplets ($d_{L0} \leqslant 5$–8 μm) undergo non-equilibrium evaporation, and the heat-transfer intensification ratio in this range of particle sizes displays no dependence on the drop diameter.

5. Comparison with experimental data

The numerical results of the present study were compared with the experimental data of [6,7]. The most detailed data were reported by Hishida et all. [5,6]. Hishida et al. studied heat transfer from a vertical flat isothermal plate in a laminar mist flow. The arithmetical mean diameter of water drops in the free flow was in the range 34–38 μm; and the mean concentration of the liquid phase was insignificant, $M_{L0} < 2.5\%$. The experimental conditions used were in line with those assumed in our calculation model: the slippage between the phases and the deposition of drops onto the wall were negligible, the surface was isothermal, the distribution of drops over sizes in the free flow was unchanged, etc.

The predicted and experimental values were compared in the form suggested by Hishida et all. [6]; namely, the heat transfer intensification ratio was considered as a function of thermal and flow parameters.

The Nu/Nu_A vs Re_x dependencies for various flow velocities are shown in Fig. 7. As is seen, with increasing Reynolds number, the rate of heat transfer in the mist flow also increases, in line with predicted data (see Figs. 5 and 6). At the same time, at a fixed Re_x number, the local heat-transfer intensification ratio also increases with increasing approach-flow velocity. As follows from Fig. 8, the increase in the heat transfer rate due to the increasing flow velocity is rather appreciable. Apparently, the Reynolds number is not the only governing parameter, and many other thermal and gas-dynamic parameters are exerting substantial influence. The latter is a factor that brings about a functional dependence of the local heat-transfer rate in the gas–drops flow both on

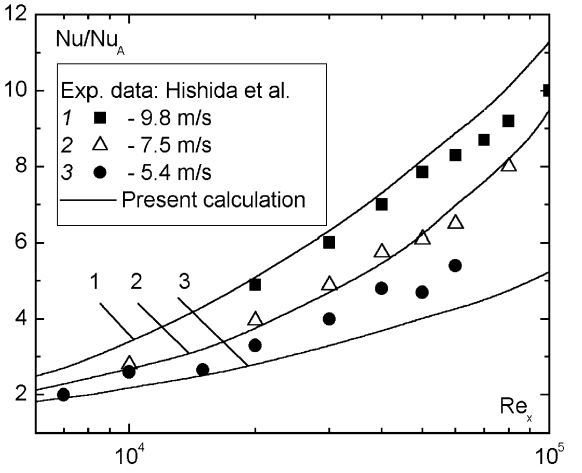

Fig. 7. Comparison between the predicted dependences and the experimental data of [6]. Effect of Reynolds number and flow velocity on local heat transfer.

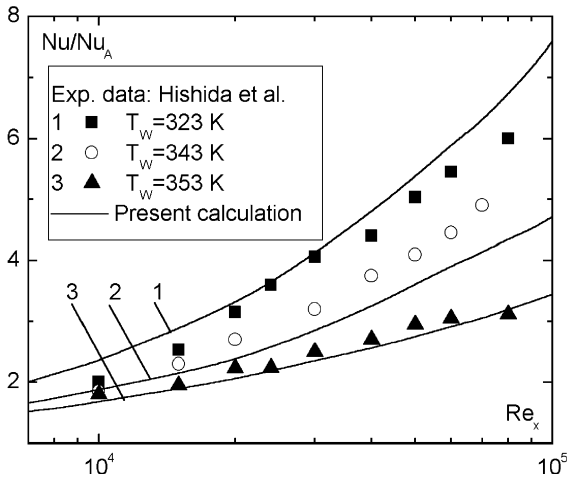

Fig. 8. Heat transfer in the gas–drop flow at various wall temperatures. Lines and symbols are the predicted data and the experimental data of [6], respectively.

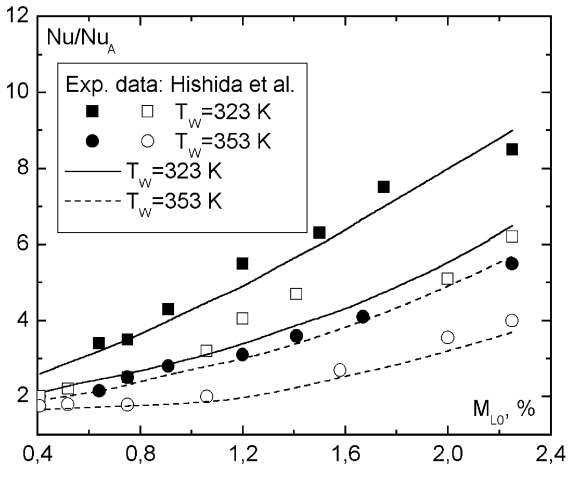

Fig. 9. Effect of drop concentration on the heat-transfer intensification ratio. Lines and symbols are the predicted data and the experimental data of [6], respectively: closed symbols – $U_0 = 9.8$ m/s; open symbols – $U_0 = 5.4$ m/s.

the Re_x number and on the flow velocity or longitudinal coordinate.

The effect of the temperature of the heat exchanging surface on the heat-transfer intensification ratio is illustrated by Fig. 8. The main conclusion that follows from the data shown is the following: as the temperature increases, the heat transfer rate diminishes rather appreciably. This decrease cannot be understood as resulting from a decrease in the density of the steam–gas phase near the heat exchanging surface, which for a laminar flow is proportional to $(T_W/T_0)^{-0.01}$ [17]. It is steam release from evaporating liquid drops that determines the physical phenomenon of interest. An increase in the surface temperature leads to rapid formation of a steam film that subsequently acts as a kind of buffer between the wall and the two-phase flow core. Such behavior of the heat-transfer rate with changing temperature factor was previously reported in many experimental studies [1–6,10].

The effect of mass concentration of liquid drops on local heat transfer can be analyzed using the data of Fig. 9. As follows from this figure, rather substantial heat transfer intensification ratios can be achieved even at low liquid contents in the flow. For instance, for the mass concentration of water drops $M_{L0} \approx 2.5\%$, the heat flux increases by 5–7 times, depending on particular experimental conditions used.

It can be concluded from Figs. 7–9 that the values predicted by the present model describe the experimental data rather adequately. The latter provides indication for the fact that, in spite of the use of many simplifying assumptions, the present model rather accurately describes the main regularities of thermal and gas-dynamic processes in a gas–drop boundary-layer flow. Apparently, the present theoretical analysis given in the present work cannot be considered as a complete one since it ignores many other possibly acting factors listed above. In a number of actual cases, the influence of these factors may be rather substantial.

Fig. 10 compares the numerical data obtained in the present study with the experimental data reported by Heyt and Larsen [7]. According to Heyt and Larsen, heat-transfer intensification effects due to evaporation should be less pronounced compared to the experimental data of [7] or the present calculations. Besides, the Nu_x vs Re_x dependence for the two-phase regime turned

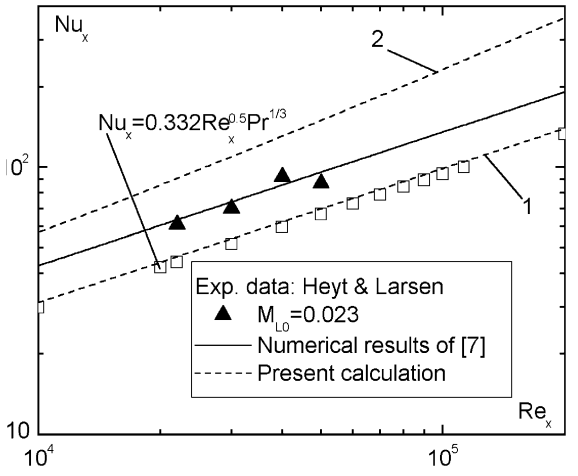

Fig. 10. Comparison between the predicted data of the present study with the experimental and theoretical data of [7]: curve 1 – $M_{L0} = 0.01$; curve 2 – $M_{L0} = 0.023$.

out to be equidistant to the law of heat transfer for a single-phase flow [20]. The reasons for the regularities observed in [7] for the gas–drop flow are still lacking clear understanding. There are many factors that could suppress the heat-transfer intensification effect in [7]; among such factors are scatter of drops over sizes, their deposition onto the channel wall, etc.

6. Conclusions

A physical model for combined heat and mass transfer in a laminar gas–steam–drop flat plate flow is developed. In this model, the liquid drops act as local sources of vapor mass and sinks of heat. A closed system of transfer equations is composed, which includes the energy equation with a source term, diffusion equation for the vapor–gas mixture with a source, and heat- and mass-transfer equation for an individual drop.

A numerical study of heat and mass transfer in a laminar two-phase vapor–drop flow is performed for various thermal and gas-dynamic parameters in the flow core.

An increase in the liquid phase concentration is shown to intensify heat transfer compared to a single-phase air flow. Comparison between the predicted and measured data shows good agreement between theoretical and experimental values.

Acknowledgements

This work was supported by the Russian Foundation for Fundamental Research (grant 01-02-16994) and by the Ministry of Education of the Russian Federation (grant TOO-1.2-260).

References

[1] M.E. Goldstein, W.-J. Yang, J.A. Clark, Momentum and heat transfer in laminar flow: a gas with liquid-droplet suspension over a circular cylinder, ASME J. Heat Transfer 89 (2) (1967) 185–193.

[2] J.W. Hodgson, R.T. Saterbak, J.E. Sunderland, An experimental investigation of heat transfer from a spray-cooled isothermal cylinder, ASME J. Heat Transfer 90 (4) (1968) 457–463.

[3] P.G. Kosky, Heat transfer to saturated mist flow in normally to heated cylinder, Int. J. Heat Mass Transfer 19 (5) (1976) 539–543.

[4] T. Aihara, M. Taga, T. Haraguchi, Heat transfer from a uniform heat flux wedge in air–water mist flow, Int. J. Heat Mass Transfer 22 (1) (1979) 51–60.

[5] K. Hishida, M. Maeda, S. Ikai, Heat transfer in two-component mist flow: boundary layer structure on an isothermal plate, in: U. Grigull, E. Hahne, K. Stefan, J. Straub (Eds.), Proceedings of the Seventh International Conference of Heat Transfer, vol. 5, Hemisphere, Washington, DC, 1982, pp. 301–306.

[6] K. Hishida, M. Maeda, S. Ikai, Heat transfer from a flat plate in two-component mist flow, ASME J. Heat Transfer 102 (3) (1980) 513–518.

[7] J.W. Heyt, P.S. Larsen, Heat transfer to binary mist flow, Int. J. Heat Mass Transfer 14 (9) (1971) 1395–1405.

[8] S.-Ch. Yao, A.G. Rane, Heat transfer of laminar mist flow in tubes, ASME J. Heat Transfer 102 (4) (1980) 678–683.

[9] V.I. Terekhov, M.A. Pakhomov, A.V. Chichindaev, Heat transfer at laminar developed flow of a vapor/drops flow in a pipe, Thermophys. Aeromech. 7 (4) (2000) 523–536.

[10] K. Mastanaiah, E.N. Ganic, Heat transfer in two-component dispersed flow, ASME J. Heat Transfer 103 (2) (1981) 300–306.

[11] V.I. Terekhov, M.A. Pakhomov, A.V. Chichindaev, Effect of evaporation of liquid droplets on the distribution of parameters in a two-species laminar flow, J. Appl. Mech. Tech. Phys. 41 (6) (2000) 1020–1028.

[12] M. Trela, An approximate calculation of heat transfer during flow of an air–water mist along heated flat plate, Int. J. Heat Mass Transfer 24 (4) (1981) 749–755.

[13] A.V.Chichindaev, Investigation of heat transfer to a cold flow of water aerosol, Ph.D. Thesis, Novosibirsk State Technical University, Novosibirsk, Russia, 1998.

[14] A.V. Lyikov, in: The Theory of Thermal Conduction, Vysshaya Shkola, Moscow, 1967, p. 231 (in Russian).

[15] C.T. Crowe, Review: Numerical models for dilute gas-particles flows, ASME J. Fluid Eng. 104 (3) (1982) 297–303.

[16] V.I. Terekhov, M.A. Pakhomov, A.V. Chichindaev, Heat and mass transfer in a developed turbulent two-component gas–vapor and droplet flow, J. Eng. Phys. Thermophys. 74 (2) (2001) 56–61.

[17] S.I. Isaev et al., in: A.I. Leont'ev (Ed.), Theory of Heat and Mass Transfer, Publishing House of Bauman Moscow State Technical University, Moscow, 1997 (in Russian).

[18] M.C. Yuen, L.W. Chen, Heat transfer measurements of evaporating liquid droplets, Int. J. Heat Mass Transfer 21 (5) (1978) 537–542.

[19] J.D. Anderson Jr. et al., in: J.F. Wendt (Ed.), Introduction to Computational Fluid Dynamics, Springer, Berlin, 1992, pp. 112–113, 170–172.

[20] H. Schlichting, Boundary Layer Theory, McGraw-Hill, New York, 1979.